

**STUDIES ON GRAPHENE BASED POLY(METHYL  
METHACRYLATE) NANOCOMPOSITES**

**SANDEEP NATH TRIPATHI**



**CENTRE FOR POLYMER SCIENCE AND ENGINEERING  
INDIAN INSTITUTE OF TECHNOLOGY DELHI**

**APRIL 2015**

© Indian Institute of Technology Delhi (IITD), New Delhi, 2015

**STUDIES ON GRAPHENE BASED POLY(METHYL  
METHACRYLATE) NANOCOMPOSITES**

by

**SANDEEP NATH TRIPATHI**

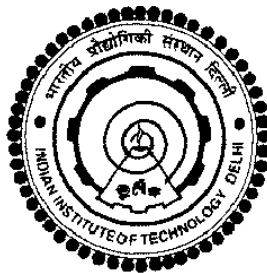
*Centre for Polymer Science and Engineering*

*submitted*

*in fulfilment of requirements of the degree of*

**Doctor of Philosophy**

**to the**



**INDIAN INSTITUTE OF TECHNOLOGY DELHI**

**APRIL 2015**

---

**Dedicated to my parents**  
**Shri Haridwar Nath Tripathi**  
**&**  
**Smt. Ramrati Devi**

## **CERTIFICATE**

This is to certify that thesis entitled “**Studies on Graphene Based Poly(methyl methacrylate) Nanocomposites**” being submitted by **Mr. Sandeep Nath Tripathi** to the Indian Institute of Technology, Delhi, for the award of degree of **Doctor of Philosophy** is a record of bonafide research carried out by him. **Mr. Sandeep Nath Tripathi** has worked under my supervision and has fulfilled the requirements for the submission of this thesis, which to my knowledge has reached the requisite standard.

The results contained in this thesis are original and have not been submitted, in part or full, to any other University or Institute for the award of any other degree or diploma.

**Date:**

**Dr. Veena Choudhary**

**Place:**

Professor

Centre for Polymer Science & Engineering

Indian Institute of Technology, Delhi

Hauz Khas, New Delhi-110016

## ACKNOWLEDGEMENTS

This thesis could have not been completed without the generosity and support of many. First of all I wish to express my heartiest gratitude to my supervisor, Prof (Mrs) Veena Choudhary for her invaluable guidance and constant encouragement. Her caring attitude like mother and co-operation has been monumental throughout my research. Through her wealth of knowledge, direction and leadership I have been able to expand my knowledge in many areas of polymer science.

I express my sincere thanks to Prof S.N. Maiti, Prof A.K. Ghosh, Dr Josemon Jacob, Dr B.K. Satapathy and Prof Manjeet Jassal for their constant encouragement, advice and support throughout my research work.

My special thanks to Mr Surender Kumar Sharma, Mr Shivkant, Mr Ashok Kapoor, Mr Virender Kumar Sharma (from glass blowing workshop), Mr Keshav Dev and Mr Alok Yadav (from NMR lab), Mr D.C. Sharma and Mr Kuldeep Sharma (from SEM lab) and office staff Ms Shalini, Sudhir, Raj and Pramod for their immediate help whenever needed.

I express my thanks to Prof B.D. Gupta from Physics Department, IIT Delhi, Dr S.K. Dhawan and Dr R.B Mathur of National Physical Laboratory Delhi, India for providing facilities to carry out experiments in their lab.

Nothing could have been accomplished without my family support. I would like to extend my special gratitude to my family for their love, support and encouragement. I am extremely thankful to my brothers Mr Dilip Nath Tripathi and Mr Amrendra Nath Tripathi for their constant encouragement and emotional support throughout my career.

I am extremely thankful to all my friends and colleagues Mr. Rajender Singh Malik, Mr Harjeet Singh Jaggi, Mrs Meenakshi Verma, Mr Pawan Verma, Ms Bhavna Sharma, Mrs Shilpi Sharma, Mrs Savita Meena, Mrs Bindu Manchanda, Mrs Achla Tripathi, Mr Debanga Konwar, Mr Sampat S. Chauhan, Mr Vishwa Pratap Singh, Ms Banpreet Kaur, Ms Pragati,

Mrs Priyanka Singh, Mrs Manisha Tomar, Dr Hemlata, Mr Rajendra Singla, Mr Abhishek Kumar, Mr Tahir Zafar and Mr Devendra Mogha and also my seniors Dr Bhanu P. Singh, Dr Parveen Saini, Dr Deeksha Gupta, Dr Anju Gupta, Dr Pravin Kumar Srivastav, Dr Shveta Mahajan and Dr Prabhat Garg.

I am also thankful to friends from other departments Dr Deepak Tripathi, Dr Navin Kumar Dwivedi, Dr Gaurav Kumar Singh (IAS), Dr Udit Kumar Soni, Dr Vinod Kumar, Mr Satyendra Kumar Mishra, Mr Manu Dalela, Mr Dinesh Shukla, Mr Abhishek Gandhi and Mr Vineet Chaudhary.

My dear friends Dr Anupam Gupta, Mr Narendra Kumar Mishra, Mr Alok Agrahari, Mr Ashwani Kumar Singh, Dr Deepak Kumar Yadav, Mr Upendra Pratap Singh and Mr Parvej Alam are greatly thanked for being an incredible support system and their encouraging words throughout my PhD.

I gratefully acknowledge University Grant Commission (UGC), India for providing Junior and Senior Research Fellowships.

Finally, I thank the 'ALMIGHTY GOD' for his blessings and further seek him to provide me blessings, patience and strength to accomplish newer goals.

Sandeep Nath Tripathi

## ABSTRACT

Over the last two decades polymer nanocomposites have been the subject of intense research interest in academia and industry which is spawned by advances such as the discovery of spherical fullerenes and carbon nanotubes. Graphene has been incorporated into various types of polymer matrices due to the exceptionally unique combination of properties such as high electrical and thermal conductivity, high surface area, strength toughness and stiffness. It was therefore expected that the incorporation of graphene into the polymer matrices will improve its mechanical, electrical, thermal and gas barrier properties. A number of thermosetting and thermoplastics have been used as matrix for the preparation of graphene/polymer nanocomposites and poly(methyl methacrylate) [PMMA] is one of them. It is used because of its some specific advantages such as low cost, optical clarity, ease of melt processibility, mould-ability mostly into any shape, good weather-ability and good physico-chemical properties. The present study was carried out to investigate the effect of reduced graphene oxide (RGO)/graphene-carbon nanotubes (GCNT) content and its method of incorporation on the properties of PMMA. These composites were characterized for thermal, electrical, mechanical, rheological, morphological properties and evaluated as gas sensor based on surface plasmon resonance utilizing fiber optic probe.

The thesis has been divided into six chapters. **Chapter 1** deals with the brief introduction of polymer nanocomposites and various nanofillers of carbon family along with detailed study of graphene followed by comprehensive literature review on the synthesis, characterization and applications of graphene in the field of polymer composites. It also reviews the different processing techniques used to fabricate polymer nanocomposites and their characterization [thermal, mechanical and electrical properties]. The basics of gas

sensors based on surface plasmon resonance utilizing fiber optic probe, the role of graphene and PMMA have also been included in this chapter.

The detailed experimental methods used for the preparation of reduced graphene oxide (RGO)/graphene-carbon nanotube (GCNT) hybrids and PMMA/RGO or PMMA/GCNT composites are given in **chapter 2** of thesis. The different techniques used for characterization and evaluation of the properties of PMMA/RGO or PMMA/GCNT composites are also described in this chapter.

The effect of reduced graphene oxide content and its method of incorporation by three methods on the properties of PMMA in PMMA/RGO composites are given in **chapter 3**. The interaction of RGO with PMMA matrix was investigated using FT-IR, Raman spectroscopy and also by X-ray diffraction analysis. The effect of RGO content on thermal, mechanical and electrical properties of PMMA/RGO nanocomposites fabricated by three different techniques, i.e. (i) *in situ* polymerization of MMA in presence of RGO (ii) *in situ* polymerization of MMA in presence of RGO and commercial PMMA beads and (iii) *in situ* polymerization of MMA in presence of RGO followed by sheet casting; up to 2.0 wt% RGO loading was investigated and the results are summarized in this chapter. Thermal stability of PMMA enhances upon incorporation of RGO in PMMA matrix irrespective of the methods. However, the mass loss in first step, which may be due to the weak linkages such as head to head linkages decreased in case of sheet casting method as compared to other two methods. It was found that for a given RGO content, all three samples give different electrical conductivity highlighting the importance of compounding method. It was found that, conductivity of composites at 0.5 wt% RGO was  $3.8 \times 10^{-6}$  S/cm (for *in situ* polymerized),  $4.1 \times 10^{-6}$  S/cm (for *in situ* polymerized in presence of PMMA beads) which is ~ 5-order higher than neat PMMA ( $2.4 \times 10^{-11}$  S/cm) and  $9.5 \times 10^{-5}$  S/cm (for samples prepared by sheet

casting method) i.e. 6-orders higher of magnitude than PMMA. The mechanical properties of PMMA/RGO showed that addition of RGO leads to improvement of modulus which indicates the increase in stiffness of the composite. Further, the tensile strength of composites show that addition beyond 1 wt% loading of RGO, leads to deterioration of mechanical strength that can be attributed to the filler agglomeration effect and poor stress transfer characteristics. The elongation decreased with increasing RGO content indicating brittle fracture of composites. These studies clearly show that all the properties were better in case of sheet casting method and hence for further studies (i.e. for melt rheology and gas sensing behaviour) all the samples were prepared using sheet casting technique.

**Chapter 4** includes the preparation and characterization of graphene-CNT (GCNT) hybrid filler via chemical method for nanocomposite application by varying the weight ratio of graphene and CNT i.e. 1:2, 1:1 and 2:1 and designated as GCNT-1, GCNT-2 and GCNT-3 respectively. The composites based on these fillers at fixed concentration (1 wt%) were prepared to investigate the effect of hybrid filler nature on the properties. On the basis of thermal and electrical properties, composites based on GCNT-2 filler showed better properties as compared to composites prepared using GCNT-1 and GCNT-3. Therefore for further studies GCNT-2 have been used to prepare PMMA/GCNT nanocomposites using varying amounts of GCNT-2 and evaluated as gas sensor.

**Chapter 5** describes the evaluation of PMMA nanocomposites based on RGO/GCNT as gas sensors using surface plasmon resonance technique utilizing fiber optic probe. For the study of sensing performance of PMMA composites based on RGO/GCNT, chapter 5 was divided into two subchapters. In **chapter 5A**, we investigated the effect of RGO content on sensing behaviour. The probe was fabricated using a 24 cm length of plastic clad silica optical fibre of core diameter 600  $\mu\text{m}$  and numerical aperture 0.4. About 1 cm length of

cladding was removed from the middle portion of the fibre followed by washing with acetone and then a Cu layer of 40 nm was coated using thermal evaporation technique. The sensing layer was then deposited over the Cu layer by dip coating method. In the first part PMMA/RGO nanocomposites were evaluated for gases like NH<sub>3</sub>, H<sub>2</sub>S, Cl<sub>2</sub>, H<sub>2</sub> and N<sub>2</sub> where the composites show selectivity mainly for NH<sub>3</sub> gas. It was also found that as RGO loading increased in PMMA/RGO composite, shift in the resonance wavelength increases and a maximum shift of 35 nm at 5 wt% RGO loading in PMMA was observed. The second part of this chapter (**chapter 5B**) deals with the sensing performance of PMMA/GCNT nanocomposites for CH<sub>4</sub>, NH<sub>3</sub>, H<sub>2</sub>S, CO<sub>2</sub>, Cl<sub>2</sub>, H<sub>2</sub> and N<sub>2</sub> where nanocomposite showed selectivity for methane gas. The maximum shift of 30 nm was observed at 5 wt% GCNT loading for PMMA/GCNT nanocomposite.

The final summary and conclusions of the thesis are given in **chapter 6**. Suggestions for future work are also included in this chapter.

# CONTENTS

	<b>Page No.</b>
Certificate	i
Acknowledgements	ii
Abstract	iv
List of Figures	xv
List of Tables	xxii
<b>CHAPTER 1</b>	
<b>INTRODUCTION AND LITERATURE SURVEY</b>	<b>1-29</b>
1.1 Introduction	1
1.2 Graphene or graphene nanosheet (GNS)	3
1.2.1 Synthesis of graphene	5
(i) Chemical vapour deposition method	5
(ii) Arc discharge method	7
(iii) Unzipping of carbon nanotubes	8
(iv) Chemical method by the reduction of graphite oxide	9
(a) Chemical reduction of graphite oxide	11
(b) Thermal reduction of graphite oxide	11
1.2.2 Properties of graphene	12
1.3 Polymer/graphene nanocomposites	14
1.3.1 Fabrication/processing of polymer/graphene nanocomposites	16
(i) Solution processing or solvent casting	16
(ii) Melt processing	17
(iii) In-situ polymerization	18

1.3.2	Properties of polymer/graphene nanocomposites	19
(i)	Mechanical properties of polymer/graphene composites	20
(a)	Chemical bonding between filler and matrix	21
(b)	van der Waals bonding between filler and matrix	21
(c)	Micro-mechanical interlocking	21
(ii)	Thermal properties of polymer/graphene composite	22
(iii)	Electrical properties of polymer/graphene composites	23
1.4	Polymer/graphene composites based on graphene-carbon nanotube (GCNT) hybrid nanofillers	25
1.5	Application of polymer/graphene composites	27
1.6	Objective of the work	28
1.7	Format of the thesis	29
<b>CHAPTER - 2</b>		
<b>EXPERIMENTAL DETAILS</b>		<b>30-48</b>
2.1	Introduction	30
2.2	Experimental	30
2.2.1	Materials	30
(i)	Raw materials	30
(ii)	Preparation of reduced graphene oxide (RGO)	31
(iii)	Preparation of graphene-carbon nanotubes (GCNT) hybrid filler	33
(a)	Preparation of CNT-COOH	33
(b)	Chlorination	34
(c)	Preparation of GCNT hybrid	34
2.2.2	Preparation of PMMA/RGO composites	35

(i)	In situ polymerization of MMA in presence of RGO	35
(ii)	In situ polymerization of MMA in presence of RGO/PMMA beads	36
(iii)	In situ polymerization of MMA in presence of RGO followed by sheet casting using pre-polymer syrup	37
2.2.3	Synthesis of PMMA/GCNT nanocomposites	38
2.2.4	Characterization of graphene and graphene/CNT based PMMA nanocomposites	39
2.2.4.1	Structural characterization	39
(a)	Fourier transforms infrared spectroscopy	39
(b)	Raman spectroscopy	40
2.2.4.2	Thermal characterization	41
(a)	Thermo-gravimetric analysis (TGA)	41
(b)	Differential scanning calorimetry (DSC)	41
(c)	Dynamic mechanical analysis (DMA)	42
2.2.4.3	Electrical conductivity	42
2.2.4.4	Morphological characterization	43
(a)	Scanning electron microscopy (SEM)	43
(b)	Transmission electron microscopy (TEM)	44
(c)	Wide angle X-ray diffraction (WAXD)	44
2.2.5.5	Energy-dispersive X-Ray spectroscopy	44
2.2.4.6	Mechanical characterization	45
2.2.4.7	Rheological characterization	46
2.2.5	Evaluation of graphene based PMMA nanocomposites as gas sensor using surface plasmon resonance	46

## **CHAPTER-3**

### **PMMA/RGO COMPOSITES: EFFECT OF RGO CONTENT AND ITS**

#### **METHOD OF INCORPORATION ON THE PROPERTIES OF PMMA 49-81**

3.1	Introduction	49
3.2	Results and discussion	53
3.2.1	Characterization of GO and RGO	53
(a)	X-ray diffraction analysis	53
(b)	Energy dispersive X-ray (EDX) spectroscopy	53
(c)	Morphological analysis	55
3.2.2	Characterization of PMMA/RGO nanocomposites	56
(i)	Structural characterization	56
(a)	Fourier transforms infra red spectroscopy	56
(b)	Raman spectroscopy	58
(ii)	X-ray diffraction analysis	59
(iii)	Electrical conductivity	60
(iv)	Thermogravimetric analysis (TGA)	63
(v)	Dynamic mechanical analysis	65
(vi)	Mechanical properties	68
(vii)	Morphological characterization	70
(viii)	Rheological characterization of PMMA/RGO nanocomposites	72
3.3	Conclusions	80

## **CHAPTER-4**

### **PMMA/GRAPHENE-CARBON NANOTUBES (GCNT) HYBRID**

#### **FILLER NANOCOMPOSITES 82-112**

4.1	Introduction	82
4.2	Results and Discussion	86
4.2.1	Characterization of GCNT hybrid filler	86
(i)	Fourier transforms infrared spectroscopy	86
(ii)	Raman Spectroscopy	87
(iii)	X-ray diffraction analysis	88
(iv)	Morphological analysis of GCNTs hybrid filler	89
(v)	Thermogravimetric analysis	91
(vi)	Electrical conductivity	93
4.2.2	Characterization of PMMA/GCNT nanocomposite	95
(i)	Structural characterization	95
(a)	FT-IR analysis	95
(b)	Raman Spectroscopy	96
(ii)	Thermal analysis	97
(a)	Thermogravimetric analysis	97
(b)	Differential scanning calorimetry	98
(c)	Dynamic mechanical analysis	100
(iii)	Electrical conductivity	104
(iv)	Morphological analysis of PMMA/GCNT composites	106
(v)	Melt rheological behaviour of PMMA/GCNT nanocomposites	107
4.3	Conclusions	113

## **CHAPTER-5**

### **EVALUATION OF NANOCOMPOSITES AS GAS SENSORS BASED ON SURFACE PLASMON RESONANCE UTILIZING FIBER OPTIC**

<b>PROBE</b>	<b>114-151</b>
5.1 Introduction	114
<b>PART 5A: PMMA/RGO NANOCOMPOSITES AS AMMONIA GAS</b>	
<b>SENSOR</b>	<b>118</b>
5.2 Fabrication of probe	118
5.3 Experimental set up	119
5.4 Performance of SPR sensing probes	121
(i) PMMA/RGO nanocomposite coated SPR probe	121
(ii) RGO coated SPR probe	123
(iii) PMMA coated SPR probe	125
5.5 Optimization of doping concentration of RGO in PMMA matrix	126
5.6 Gas selectivity of the probes	127
5.7 Performance of different probes for ammonia gas	130
5.8 Probe reproducibility	132
5.9 Environmental effects	134
5.10 Conclusions	136
<b>PART 5B: PMMA/GCNT HYBRID COMPOSITES AS METHANE</b>	
<b>GAS SENSOR</b>	<b>137</b>
5.11 Fabrication of probe	137
5.12 Experimental set up	138
5.13 Performance of SPR probes	138
(i) PMMA/GCNT nanocomposite coated SPR probe	138
(ii) RGO coated SPR probe	141
(iii) CNT coated SPR spectra	142
(iv) GCNT coated SPR probe	143

(v)	PMMA coated SPR probe	145
5.14	Optimization of the PMMA/GCNT nanocomposite sensing probe	146
5.15	Gas selectivity of the probes	147
5.16	Performance of different probes for methane gas	149
5.17	Reason for response of the probe (PMMA/GCNT) towards methane gas	150
5.18	Conclusions	151
<b>CHAPTER- 6</b>		
<b>SUMMARY, CONCLUSION AND FUTURE SCOPE</b>		<b>152-164</b>
6.1	Introduction	152
6.2	Preparation and characterization of RGO	153
6.3	Preparation and characterization of PMMA/RGO composites	154
6.4	Preparation and characterization of PMMA/GCNT hybrid nanocomposites	158
6.4.1	Synthesis and characterization of GCNT hybrid filler	158
6.4.2	Preparation and characterization of PMMA/GCNT hybrid nanocomposites	159
6.5	Evaluation of PMMA/RGO and PMMA/GCNT hybrid composites as gas sensors based on surface plasmon resonance utilizing fiber optic probe	161
6.5.1	PMMA/RGO composites as ammonia gas sensor	161
6.5.2	PMMA/GCNT hybrid composites as methane gas sensor	161
6.6	Conclusions	162
6.7	Suggestions for future work	163
<b>REFERENCES</b>		<b>165-191</b>

## List of Figures

	Page No.
<b>Figure 1.1:</b> Molecular structure of graphene as $sp^2$ hybridized chicken wire pattern	3
<b>Figure 1.2:</b> Graphene as building block of all graphitic forms	4
<b>Figure 1.3:</b> Schematic diagram of growth of graphene on $SiO_2$ substrates in CVD process	6
<b>Figure 1.4:</b> Schematic diagram of D.C. arc discharge set up	7
<b>Figure 1.5:</b> Pictorial representation for sequential unzipping of a carbon nanotube to graphene nanoribbons	8
<b>Figure 1.6:</b> Schematic representation from graphite to graphite oxide.	9
<b>Figure 1.7:</b> Schematic representation of reduction of graphite oxide to reduced graphene oxide	10
<b>Figure 1.8:</b> Sheet of graphene rolled to show formation of different types of single walled carbon nanotube	12
<b>Figure 1.9:</b> Schematic of the formation of PMMA/GO nanocomposite by ATRP	19
<b>Figure 2.1:</b> Chemical structure of AIBN, MMA monomer and PMMA	31
<b>Figure 2.2:</b> Schematic for the preparation of graphene oxide (GO) and reduced graphene oxide (RGO)	32
<b>Figure 2.3:</b> Schematic representation for the preparation of GCNT hybrid filler	33
<b>Figure 2.4:</b> Mechanism for the catalysis of DMF in chlorination	34
<b>Figure 2.5:</b> Pictorial view of PMMA/RGO nanocomposites preparation method (1) in-situ (2) in presence of PMMA beads and (3) sheet	

	casting	35
<b>Figure 2.6:</b>	Schematic for the fabrication of PMMA/GCNT hybrid composites	38
<b>Figure 2.7:</b>	Experimental set up of SPR probe for gas sensing utilizing optical fiber	48
<b>Figure 3.1:</b>	X-ray diffraction patterns of graphite, graphene oxide (GO) and reduced graphene oxide (RGO)	54
<b>Figure 3.2:</b>	SEM-EDX images of (a) graphene oxide (GO) and (b) reduced graphene oxide (RGO)	55
<b>Figure 3.3:</b>	(a) SEM (b) TEM and (c) AFM images of RGO	56
<b>Figure 3.4:</b>	FTIR spectra of (a) graphite, (b) graphene oxide (GO), (c) graphene (RGO), (d) PMMA and (e) PMMA/RGO composite (1 wt%)	57
<b>Figure 3.5:</b>	Raman spectra of (a) graphite (b) GO (c) RGO (d) PMMA/RGO (1 wt%) and (e) PMMA/RGO composite (2 wt%)	59
<b>Figure 3.6:</b>	XRD patterns of GO, RGO, PMMA and PMMA/RGO composites (2 wt%) and (1 wt%)	60
<b>Figure 3.7:</b>	Effect of RGO content on the electrical conductivity of PMMA/RGO nanocomposites	61
<b>Figure 3.8:</b>	TG traces of (a) graphite, graphene oxide (GO) and RGO; RGO and PMMA/RGO composites (b) in situ method (c) in presence of PMMA beads (d) sheet-casting method	63
<b>Figure 3.9:</b>	Plot of storage modulus ( $E'$ ) vs temperature for PMMA/RGO composites prepared by three methods [In situ- Method 1; PMMA Beads- Method 2 and PMMA/RGO- Method 3]	66

<b>Figure 3.10:</b>	Plot of loss modulus ( $E''$ ) vs temperature for PMMA/RGO composites prepared by three methods [In situ- Method 1; PMMA Beads- Method 2 and PMMA/RGO- Method 3]	68
<b>Figure 3.11:</b>	Variation of (a) tensile modulus (b) tensile strength and (c) strain at break with RGO content	69
<b>Figure 3.12:</b>	SEM images of (a) fracture surface of PMMA; PMMA/RGO nanocomposite (1 wt%) (b) in situ (c, d) in presence of PMMA beads, (e, f) Sheet casting	71
<b>Figure 3.13:</b>	HRTEM images of RGO (a, b) PMMA/RGO composite (1 wt%) (c, d) in situ (e, f) sheet casting	72
<b>Figure 3.14:</b>	Amplitude sweep test of PMMA and PMMA/RGO nanocomposites	73
<b>Figure 3.15:</b>	Plots of (a) storage modulus ( $G'$ ) (b) loss modulus ( $G''$ ) and (c) complex modulus ( $G^*$ ) of PMMA/RGO nanocomposites as a function of frequency	75
<b>Figure 3.16:</b>	Plots of $G'$ , $G''$ vs frequency for PMMA/RGO nanocomposites	76
<b>Figure 3.17:</b>	Complex viscosities as a function of (a) frequency and (b) RGO content for PMMA/RGO nanocomposites	79
<b>Figure 3.18:</b>	SEM and TEM of PMMA/RGO nanocomposites (a, d) 0.5 wt% (b, e) 2.0 wt% (c, f) 5.0 wt%	80
<b>Figure 4.1:</b>	IR spectra of (a) CNT-COOH (b) GO (c) RGO (d) GCNT-1 and (e) GCNT-2	87
<b>Figure 4.2:</b>	Raman spectra of (a) GO (b) CNT-COOH (c) RGO (d) GCNT-1 and (e) GCNT-2	88
<b>Figure 4.3:</b>	X-ray diffraction pattern of GO, RGO, MWCNT, GCNT-1 and	89

	GCNT-2	
<b>Figure 4.4:</b>	SEM micrographs of (a) RGO (b) MWCNT (c) GCNT-1 and (d) GCNT-2	90
<b>Figure 4.5:</b>	TEM micrographs of (a) RGO (b) MWCNT (c) GCNT-1 and (d) GCNT-2	91
<b>Figure 4.6:</b>	TG traces of (a) GCNTs hybrid fillers (b) PMMA composites at 1 wt% of filler (RGO, GCNTs and CNT)	93
<b>Figure 4.7:</b>	IR spectra of (a) RGO (b) GCNT-2 (c) PMMA and (d) PMMA/GCNT nanocomposite (1 wt%)	95
<b>Figure 4.8:</b>	Raman spectra of GCNT, PMMA and PMMA/GCNT nanocomposite of varying GCNT content (1.0, 1.5 and 3.0 wt%)	96
<b>Figure 4.9:</b>	(a) TG (b) DTG traces of PMMA and PMMA/GCNT hybrid nanocomposites	98
<b>Figure 4.10:</b>	DSC scans of PMMA and PMMA/GCNT nanocomposites of varying GCNT content	99
<b>Figure 4.11:</b>	Variation of (a) storage (b) loss modulus and (c) tan delta of PMMA and PMMA/GCNT nanocomposites with temperature	102
<b>Figure 4.12:</b>	Effect of GCNT content in PMMA/GCNT nanocomposites on the electrical conductivity	105
<b>Figure 4.13:</b>	SEM micrographs of PMMA and PMMA/GCNT nanocomposites	106
<b>Figure 4.14:</b>	Plot of (a) storage modulus ( $G'$ ) (b) loss modulus ( $G''$ ) and (c) tan delta vs frequency for PMMA and PMMA/GCNT nanocomposites	109
<b>Figure 4.15:</b>	Plot of complex viscosity as a function of (a) angular frequency	110

(b) GCNT content at varying frequency for PMMA and PMMA/GCNT nanocomposites

- Figure 4.16:** Comparison of Storage modulus ( $G'$ ) and loss modulus ( $G''$ ) vs frequency for the composite containing (a) 0.5 wt% (b) 2.0 wt% of RGO and GCNT 112
- Figure 4.17:** Complex viscosity of PMMA composite containing 0.5 wt% and 2.0 wt% of GCNT and RGO respectively 112
- Figure 5.1:** Schematic diagram of the experimental set up of fiber optic SPR probe for ammonia gas sensing 120
- Figure 5.2:** (a) SPR spectra for different concentrations of ammonia gas (b) variation of resonance wavelength with concentration of ammonia gas for copper and PMMA/RGO nanocomposite (5 wt%) coated fiber optic SPR probe 122
- Figure 5.3:** (a) SPR spectra for different concentrations of ammonia and (b) variation of resonance wavelength with concentration of ammonia gas for copper and RGO coated fiber optic SPR probe 125
- Figure 5.4:** (a) SPR spectra for different concentrations of ammonia (b) variation of resonance wavelength with concentration of ammonia gas for copper and PMMA coated fiber optic SPR probe 126
- Figure 5.5:** Variation of total shift in resonance wavelength with RGO loadings in PMMA matrix for ammonia gas concentration ranging from 10-100 ppm for copper/(PMMA/RGO) nanocomposite coated fiber optic SPR probe 127
- Figure 5.6:** Total shift in the resonance wavelength for the concentration

	range 10-100 ppm of different gases with (a) RGO and (b) PMMA/RGO nanocomposite (5 wt%) as a sensing layer	129
<b>Figure 5.7:</b>	(a) Total shift in resonance wavelength for ammonia gas concentration range from 10-100 ppm and (b) variation of sensitivity with concentration of ammonia gas for three different sensing probes	131
<b>Figure 5.8:</b>	Total shift in resonance wavelength of PMMA/RGO nanocomposite (5 wt%) sensing layer for the concentration range 10–20 ppm of different gases	132
<b>Figure 5.9:</b>	Variation of the normalized transmitted power with time as the gas is introduced and removed from the gas chamber at NH <sub>3</sub> gas concentration 20 ppm and wavelength of light is 882 nm	133
<b>Figure 5.10:</b>	Possible interaction of NH <sub>3</sub> molecules with RGO nanosheets	135
<b>Figure 5.11:</b>	Schematic of fabricated probe using different sensing layers	138
<b>Figure 5.12:</b>	(a) SPR spectra for different concentrations of methane gas (b) variation of resonance wavelength with concentration of methane gas for silver and PMMA/GCNT hybrid nanocomposite (5 wt%) coated fiber optic SPR probe	140
<b>Figure 5.13:</b>	(a) SPR spectra for different concentrations of methane and (b) variation of resonance wavelength with concentration of methane gas for silver and RGO coated fiber optic SPR probe	142
<b>Figure 5.14:</b>	(a) SPR spectra for different concentrations of methane and (b) variation of resonance wavelength with concentration of methane gas for silver and CNT coated fiber optic SPR probe	143
<b>Figure 5.15:</b>	(a) SPR spectra for different concentrations of methane and (b)	144

	variation of resonance wavelength with concentration of methane gas for silver and GCNT coated fiber optic SPR probe	
<b>Figure 5.16:</b>	(a) SPR spectra for different concentrations of methane and (b) variation of resonance wavelength with concentration of methane gas for silver and PMMA coated fiber optic SPR probe	146
<b>Figure 5.17:</b>	Variation of total shift in resonance wavelength with GCNT loadings in PMMA matrix for methane gas concentration ranging from 10-100 ppm for silver-PMMA/GCNT hybrid nanocomposite coated fiber optic SPR probe	147
<b>Figure 5.18:</b>	Total shift in the resonance wavelength for the concentration range 10-100 ppm of different gases with (a) RGO and (b) CNT (c) GCNT and (d) PMMA/GCNT hybrid nanocomposite (5 wt%) as a sensing layer	149
<b>Figure 5.19:</b>	(a) Total shift in resonance wavelength for methane gas concentration 10-100 ppm and (b) variation of sensitivity with concentration of methane gas for different sensing probes	150
<b>Figure 6.1:</b>	Schematic for the preparation reduced graphene oxide (RGO) from graphite	154
<b>Figure 6.2:</b>	Schematic for the preparation PMMA/RGO composites by three methods using in-situ bulk polymerization technique	155
<b>Figure 6.3:</b>	Schematic for the preparation of GCNT hybrid filler	158

## List of Tables

	Page No.
<b>Table 2.1:</b> Properties of poly(methyl methacrylate) [from supplier data sheet]	31
<b>Table 2.2:</b> Details of PMMA/RGO composite prepared by sheet casting method alongwith sample designation	37
<b>Table 2.3:</b> Details of PMMA/GCNT hybrid composite prepared by sheet casting method alongwith sample designation	39
<b>Table 3.1:</b> Results of EDX analysis for GO and RGO	54
<b>Table 3.3:</b> Results of electrical conductivity for PMMA/RGO composites prepared by different method	62
<b>Table 3.4:</b> Results of TG traces of GO, RGO and PMMA/RGO nanocomposites in N <sub>2</sub> atmosphere	64
<b>Table 3.5:</b> Results of storage modulus and glass transition for PMMA/RGO composites	67
<b>Table 3.6:</b> Mechanical properties of PMMA/RGO composites prepared by different methods	69
<b>Table 3.7:</b> Results of crossover frequency response for PMMA and PMMA/RGO composites prepared by sheet casting	77
<b>Table 4.1:</b> Results of electrical conductivity of PMMA composite having different fillers	94
<b>Table 4.2:</b> Details of PMMA/GCNT hybrid composites prepared by sheet casting along with sample designation	94
<b>Table 4.3:</b> Results of TG traces for PMMA/GCNT nanocomposites in N <sub>2</sub> atmosphere	99

<b>Table 4.4:</b>	Results of storage modulus and glass transition temperature for PMMA/GCNT nanocomposites	101
<b>Table 4.5</b>	Results of reinforcement effectiveness parameter obtained from storage modulus vs temperature plot of PMMA/GCNT nanocomposites	103